Letters

A General Mutual Coupling Model of MIMO Capacitive Coupling Interface With Arbitrary Number of Ports

Wei Zhou, *Member, IEEE*, Liang Huang, Bo Luo, *Student Member, IEEE*, Ruikun Mai, *Senior Member, IEEE*, Zhengyou He, *Senior Member, IEEE*, and Aiguo Patrick Hu, *Senior Member, IEEE*

***Abstract*—A general mutual coupling model of multiple input and/or multiple output (MIMO) capacitive coupling interface with an arbitrary number of ports is proposed. In the model proposed in this letter, all the capacitances between the metal plates are taken into account. The self-capacitance of each port and mutual capacitances between the two ports are defined, and a simple equivalent circuit composed of self capacitances and current-controlled voltage sources is obtained. The proposed model helps to reduce the complexity of the MIMO capacitive coupling interface and can be used to simplify the analysis of the power transfer performance of MIMO capacitive power transfer systems. An example capacitive coupling interface setup with two input ports and two output ports is built and tested. The measured and model-based theoretical results of the self and mutual capacitances of the capacitive coupling interface are compared and found to be in good consistency, which verifies the correctness of the proposed model.**

***Index Terms*—Capacitive coupling interface, mutual coupling model, multi-input and/or multi-output (MIMO).**

I. Introduction

In RECENT years, the applications of wireless power transfer (WPT) are gradually increasing in high-power, dynamic, and multiload WPT scenarios, as follows.

1) For high-power WPT systems, due to the limitation of voltage–ampere (*V-A*) rating and cost of power electronic components, multiple pairs of coupling interfaces can be used to transfer power in parallel to reduce the *V–A* stress on components [1], [2].

Manuscript received August 9, 2020; revised October 1, 2020; accepted October 24, 2020. Date of publication October 28, 2020; date of current version February 5, 2021. This work was supported in part by the National Natural Science Foundation of China under Grant 51907170 and in part by the Fundamental Research Funds for the Central Universities under Grant 2682019CX24. *(Corresponding author: Ruikun Mai.)*

Wei Zhou, Bo Luo, Ruikun Mai, and Zhengyou He are with the School of Electrical Engineering, Southwest Jiaotong University, Chengdu 610031, China (e-mail: wzhou@swjtu.edu.cn; lb2010@my.swjtu.edu.cn; mairk@swjtu.edu.cn; hezy@swjtu.edu.cn).

Liang Huang is with the Department of Electrical and Electronic Engineering, University of Nottingham Ningbo China, Ningbo 315100, China (e-mail: liang.huang@nottingham.edu.cn).

Aiguo Patrick Hu is with the Department of Electrical and Computer Engineering, University of Auckland, Auckland 1010, New Zealand (e-mail: a.hu@auckland.ac.nz).

Color versions of one or more of the figures in this article are available online at https://ieeexplore.ieee.org.

Digital Object Identifier 10.1109/TPEL.2020.3034372

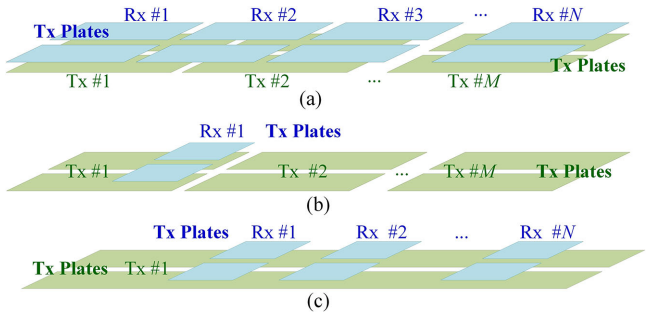

Fig. 1. Structure of MIMO capacitive coupling interfaces for applications: (a) high-power, (b) dynamic charging, and (c) multiload CPT system.

2) For dynamic WPT systems, multiple segmented coupling interfaces can be adopted at the transmitting *Tx* side to reduce the electromagnetic interference and standby loss [3], [4].
3) For multiload WPT systems, more than one coupling interfaces are often needed to supply power to individual receiving *Rx* modules [5], [6].

Up to now, most of the research works on the multiple input and/or multiple output (MIMO) coupling interfaces of WPT systems are focused on inductive power transfer systems. An alternative WPT technology named capacitive power transfer (CPT) was proposed with the advantages of reduced volume and weight of coupling interfaces as well as lower eddy current losses and effects on the surroundings, etc. [7]. As a type of WPT technology, the MIMO capacitive coupling interface, as shown in Fig. 1, has been proposed for applying the CPT technology to high-power, dynamic charging, or multiloads applications [8]–[10].

The capacitive coupling interface is composed of metal plates, which form a complicated capacitance network. The modeling of a capacitive coupling interface is an important step to simplify the system and determine the key parameters, such as self and mutual capacitances. The single-input and single-output (SISO) capacitive coupling interface was approximately modeled as two capacitors connected in series when the air gap is very small [11]. When the coupling condition becomes more complicated with

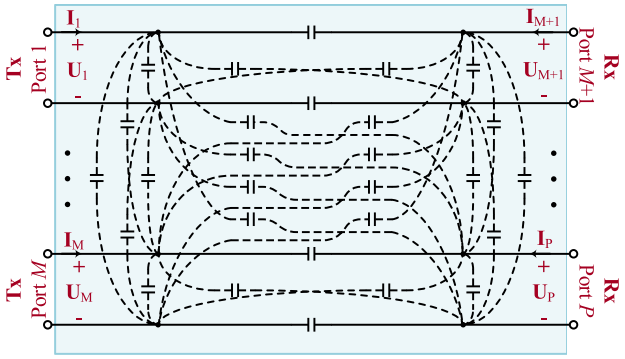

Fig. 2. Capacitances between the metal plates of the MIMO capacitive coupling interface with *M Tx* ports and *N Rx* ports.

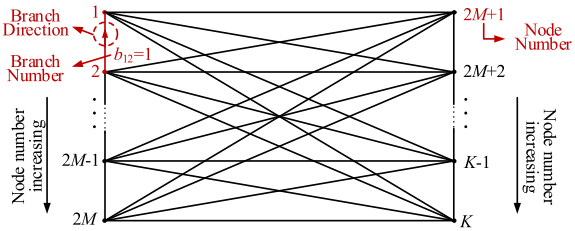

Fig. 3. Directed network of capacitive coupling interface linked by coupling plates as nodes.

larger coupling distances from millimeters to centimeters, the simple series model is not valid anymore. Huang and Hu [12] proposed a modeling method and defined a coupling coefficient to present the coupling degree by considering all the capacitances between the metal plates of a SISO capacitive coupling interface. This modeling method is adopted by Zhang *et al.* [13], [14] to realize the parametric design of a high-order compensated SISO-CPT system with a 15-cm coupling distance.

More metal plates are needed in the MIMO-CPT system with multiple coupling interfaces, which would lead to a more complicated capacitance network of the coupling interface. In addition, environmental factors, such as metal foreign objects, may couple with the coupling plates, which affect the parameters of the coupling interface. These metal foreign objects can also be treated as additional metal plates, which should be considered in the MIMO capacitive coupling interface. No research work has been reported in the literature on the modeling of MIMO capacitive coupling interfaces. The existing modeling and calculation method of the mutual capacitance and self-capacitance parameters for SISO coupling interfaces is not applicable for MIMO systems. This brings great inconvenience to the design of compensation networks and analysis of power transfer characteristics of CPT systems with MIMO capacitive coupling interfaces.

To fulfill the identified research gap, this letter proposes a method for modeling MIMO capacitive coupling interfaces with an arbitrary number of ports. Based on this model, the self-capacitance of each individual port and the mutual capacitance between any two ports can be calculated, and the complicated MIMO capacitive coupling interface can be represented by a set of equivalent subcircuits. Each subcircuit is composed of a self-capacitance and several current-controlled voltage sources (CCVSs) in series. It should be noted that the self and mutual capacitances of the ports, rather than the metal plates, are defined in this letter. The main contributions of this letter are as follows.

1) The MIMO capacitive coupling interface is generally simplified as several independent subcircuits with a capacitor and CCVS connected in series.
2) The concepts of self and mutual capacitance of MIMO capacitive coupling interface are clarified and their calculation methods proposed, which are useful for the analysis and design of CPT systems.
3) The relationship between the self/mutual capacitances and the port voltages/currents is established, so the self and mutual capacitances of a MIMO capacitive coupling interface can be indirectly obtained by measuring the port impedances, voltages, and currents, even considering additional foreign objects in the environment.

II. Modeling of MIMO-Capacitive Coupler

A circuit of the capacitive coupling interface with M *Tx* ports and N *Rx* ports is illustrated in Fig. 2. All the capacitances between the metal plates are modeled as lump capacitances. The number of ports, plates, and capacitance branches of the MIMO capacitive coupling interface are $P = M + N$, $K = 2(M + N)$, and $L = K(K-1)/2$, respectively.

If all the metal plates are regarded as nodes and all the capacitance branches are considered as directed branches, the coupling network, as shown in Fig. 2, can be transformed into a directed network, as shown in Fig. 3. Assume that all the *Tx* ports are located on the left side and the *Rx* ports are on the right side. The serial number of nodes, branches, and ports in the network, as well as the direction of each branch, are defined according to the following rules.

1) The serial number k of nodes increases from top to bottom and from left to right, where $k \in [1, K]$.
2) The serial number p of ports increases from top to bottom and from left to right, where $p \in [1, P]$.
3) The serial number of the branch between node i and j $(i < j)$ is defined as $l_{ij} = (j-i) + \prod_{s=0}^{i-1}(K-s-1)$, where $i \in [1, K-1]$, $j \in [2, K]$, and $l_{ij} \in [1, L]$.
4) The positive direction of the branch between node i and j $(i < j)$ is from node j to node i.

According to the superposition theorem, the relationship between the port voltages and port currents of the MIMO capacitive coupling interface can be expressed as a matrix equation

$$\underbrace{\begin{bmatrix} \mathbf{U}_1 \\ \vdots \\ \mathbf{U}_P \end{bmatrix}}_{\mathbf{U}} = \underbrace{\begin{bmatrix} Z_{11} \cdots Z_{1P} \\ \vdots \ddots \vdots \\ Z_{P1} \cdots Z_{PP} \end{bmatrix}}_{\mathbf{Z}} \cdot \underbrace{\begin{bmatrix} \mathbf{I}_1 \\ \vdots \\ \mathbf{I}_P \end{bmatrix}}_{\mathbf{I}} \tag{1}$$

where the impedance matrix $\mathbf{Z}$ is determined by the topology and configuration of the coupling interface. Before calculating the matrix $\mathbf{Z}$, three matrices $\mathbf{A}$, $\mathbf{Y}$, and $\mathbf{R}$ are defined as follows to simplify the modeling process.

Incidence matrix $\mathbf{A}(a_{kl})$ contains all the information of the nodes and branches connection. The row of the matrix indicates the nodes and the column represents the branches. The element $a_{kl} = 1$ (or -1) if node k is a terminal of branch l and the direction of branch l points (or does not point) to node k; $a_{kl} = 0$ if node k is not a terminal of branch l. From the element definition mentioned above, the rank of $\mathbf{A}(a_{kl})$ is K–1. Hence, the first row of the matrix is removed to ensure the matrix nonsingular. Then, the incidence matrix $\mathbf{A}(a_{kl})$ can be given as

$$\mathbf{A} = \left[\mathbf{A}_1, \cdots \mathbf{A}_k, \cdots \mathbf{A}_{K-1}\right]_{(K-1)\times L} \tag{2}$$

where $\mathbf{A}_k = \begin{bmatrix} 0_{\max\{0,k-2\}\times(K-k)} \\ -1_{(k-1)\times(K-k)} \\ \mathbf{E}_{(K-k)\times(K-k)} \end{bmatrix}$, $\mathbf{E} = \begin{bmatrix} 1 \cdots 0 \\ \vdots \ddots \vdots \\ 0 \cdots 1 \end{bmatrix}$, $1 = \begin{bmatrix} 1 \cdots 1 \\ \vdots \ddots \vdots \\ 1 \cdots 1 \end{bmatrix}$, and $0 = \begin{bmatrix} 0 \cdots 0 \\ \vdots \ddots \vdots \\ 0 \cdots 0 \end{bmatrix}$.

Admittance matrix $\mathbf{Y}(y_l)$ is constructed to describe the admittances of the branches. Define the capacitance of branch b_{ij} as C_{ij}, the matrix $\mathbf{Y}(y_l)$ can be given as

$$\mathbf{Y} = j\omega \cdot \mathbf{C}_{L\times L} = j\omega \cdot \mathrm{diag}\left[\mathbf{C}_1, \cdots \mathbf{C}_k, \cdots \mathbf{C}_{K-1}\right] \tag{3}$$

where $\mathbf{C}_k = [\, C_{k,k+1}, C_{k,k+2}, \ \ldots \ C_{k,K}\,]$, j represents the imaginary unit, ω refers to the angular frequency, and diag[$\cdot$] is the diagonal matrix operator.

Recognition matrix $\mathbf{R}(r_{pl})$ is adopted to select port branches from L branches of the directed network, where the port branch means the branch terminated by two nodes belonging to the same port (e.g., branch b_{12}, b_{34}, etc.). The row of the matrix $\mathbf{R}(r_{pl})$ represents ports and the column indicates branches. The element $r_{pl} = 1$ if branch l is the port branch of port p; otherwise $r_{pl} = 0$. Then the recognition matrix $\mathbf{R}(r_{pl})$ is expressed as

$$\mathbf{R} = \left[\mathbf{R}_1 \cdots \mathbf{R}_k \cdots \mathbf{R}_{K-1}\right]_{P\times L} \tag{4}$$

where

$$\mathbf{R}_k = \begin{bmatrix} \mathbf{0}_{(k-1)\times 1} & \\ 1 & \mathbf{0}_{P\times 2(K-k-1)} \\ \mathbf{0}_{P\times 1} & \end{bmatrix}.$$

According to (1), when an external current source of 1 A is connected to port p, where $p \in [1, P]$, and the current of other ports are zero, the port voltage $\mathbf{U}_p$ is equal to $\mathbf{Z}_p$, which is the pth column of matrix $\mathbf{Z}$. In this case, the KCL and KVL equations of the MIMO capacitive coupling interface are

$$\begin{cases} \mathbf{A}\cdot(\mathbf{I}_b - \mathbf{I}_{sp}) = 0 & \text{(KCL)} \\ \mathbf{A}^T \cdot \mathbf{U}_o = \mathbf{U}_b & \text{(KVL)} \end{cases} \tag{5}$$

where $\mathbf{I}_b = [\, I_{b1}, \ldots \ I_{bL}\,]^T$ represents the current on each branch. $\mathbf{I}_{sp}$ indicates the current of external current source connected with branches, so the elements of $\mathbf{I}_{sp}$ are all zero, except the element corresponding to the pth port branch equal one. $\mathbf{U}_b = [\, U_{b1}, \ldots \ U_{bL}\,]^T$ and $\mathbf{U}_p = [\, U_{p1}, \ldots \ U_{pP}\,]^T$ are the voltage of each branch and port, respectively. The relationship between the voltage and current on each branch satisfies

$$\mathbf{I}_b = \mathbf{Y} \cdot \mathbf{U}_b. \tag{6}$$

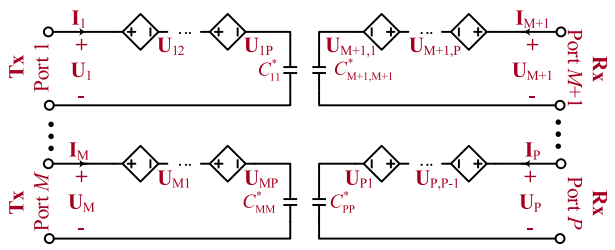

Fig. 4. Equivalent circuit of MIMO capacitive coupling interface.

Substituting (6) into (5)

$$\mathbf{U}_o = \left(\mathbf{A}\mathbf{Y}\mathbf{A}^T\right)^{-1}\mathbf{A}\mathbf{I}_{sp}. \tag{7}$$

Using the recognition matrix $\mathbf{Z}$ to select the port voltage from all branch voltages, the pth column of $\mathbf{Z}$ can be found from

$$\mathbf{Z}_p = \mathbf{R}\cdot\mathbf{U}_b = \mathbf{R}\mathbf{A}^T\left(\mathbf{A}\mathbf{Y}\mathbf{A}^T\right)^{-1}\mathbf{A}\mathbf{I}_{sp}. \tag{8}$$

Therefore, by combining the columns of $\mathbf{Z}$ matrix, the expression of $\mathbf{Z}$ is obtained as follows:

$$\begin{aligned} \mathbf{Z}\,(Z_{st}) &= \left[\mathbf{Z}_1 \cdots \mathbf{Z}_P\right] = \mathbf{R}\mathbf{A}^T\left(\mathbf{A}\mathbf{Y}\mathbf{A}^T\right)^{-1}\mathbf{A}\left[\mathbf{I}_{s1} \cdots \mathbf{I}_{sP}\right] \\ &= \mathbf{R}\mathbf{A}^T\left(\mathbf{A}\mathbf{Y}\mathbf{A}^T\right)^{-1}\mathbf{A}\mathbf{R}^T \\ &= 1/j\omega \cdot \mathbf{R}\mathbf{A}^T\left(\mathbf{A}\mathbf{C}\mathbf{A}^T\right)^{-1}\mathbf{A}\mathbf{R}^T \end{aligned} \tag{9}$$

where the elements of the matrix $\mathbf{Z}$ can be expressed as

$$Z_{st} = 1/j\omega C^*_{st} \Leftrightarrow C^*_{st} = \left[\mathbf{R}\mathbf{A}^T\left(\mathbf{A}\mathbf{C}\mathbf{A}^T\right)^{-1}\mathbf{A}\mathbf{R}^T\right]^{-1}_{st}. \tag{10}$$

In (10), C^*_{st} is the element of the capacitance matrix. When $s = t$, C^*_{st} is the self-capacitance of port s or t; otherwise, C^*_{st} is the mutual capacitance between port s and t. Then (1) can be expanded as

$$\begin{bmatrix} \mathbf{U}_1 \\ \vdots \\ \mathbf{U}_P \end{bmatrix} = \begin{bmatrix} 1/j\omega C^*_{11} & \cdots & 1/j\omega C^*_{1P} \\ \vdots & \ddots & \vdots \\ 1/j\omega C^*_{P1} & \cdots & 1/j\omega C^*_{PP} \end{bmatrix} \cdot \begin{bmatrix} \mathbf{I}_1 \\ \vdots \\ \mathbf{I}_P \end{bmatrix}. \tag{11}$$

Thus, the voltage of any port s ($s \in [1, P]$) can be expressed by the current of all ports

$$\mathbf{U}_s = \mathbf{I}_s/j\omega C^*_{ss} + \sum_{t\in[1,P]\cap t\neq s} \mathbf{U}_{st} \tag{12}$$

where $\mathbf{U}_{st} = \mathbf{I}_t/j\omega C^*_{st}$ and $1/j\omega C^*_{st}$ can be defined as the transfer impedance between the ports s and t.

Finally, the complicated coupling circuit in Fig. 2 can be simply equivalent to the circuit in Fig. 4 according to (11) and (12). Each port is connected up with an equivalent self-capacitance and $P-1$ CCVSs in series.

III. Experimental Verification

An experimental setup of a capacitive coupling interface with two *Tx* ports and two *Rx* ports was constructed, as shown in Fig. 5, where plates (P_1-P_2) and (P_3-P_4) form two *Tx* ports, and plates (P_5-P_6) and (P_7-P_8) form two *Rx* ports. All the eight

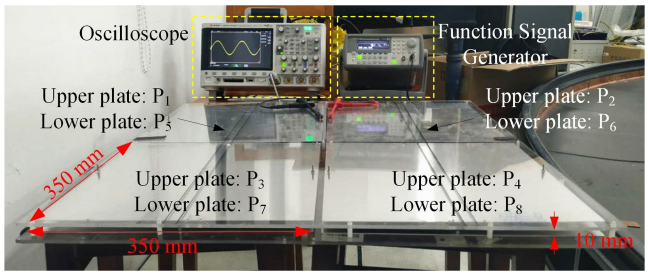

Fig. 5. Experimental setup of capacitive coupling with two inputs and two outputs.

TABLE I
COMPARISON BETWEEN MEASURED AND THEORETICAL RESULTS

Parameters	Theoretical values (pF)	Measured values (pF)					Error
		8(a)	8(b)	8(c)	8(d)	Average	
C_{11}^*	20.52			**19.77**			3.7%
C_{22}^*	20.61			**19.68**			4.5%
C_{33}^*	20.54			**19.71**			4.0%
C_{44}^*	20.64			**19.74**			4.6%
C_{12}^*	91.15	96.13	93.23	-	-	**94.68**	3.7%
C_{13}^*	24.54	22.94	-	23.12	-	**23.03**	6.1%
C_{14}^*	92.13	98.85	-	-	96.03	**97.44**	5.5%
C_{23}^*	92.09	-	94.46	99.94	-	**97.20**	5.3%
C_{24}^*	24.67	-	23.60	-	23.40	**23.50**	4.7%
C_{34}^*	91.08	-	-	95.87	98.70	**97.29**	6.4%

coupling plates are made of aluminum with the size of 350 mm $\times$ 350 mm $\times$ 1 mm. This letter verifies the proposed mutual coupling model by comparing the practically measured and model-based theoretical values of self-capacitance and mutual capacitance of the capacitive coupling interface in Fig. 5.

The capacitances between the metal plates of the coupling interface can be achieved from the finite-element method simulation software Maxwell, and the theoretical values of the self and mutual capacitances of ports can be found from (2)–(4) and (6). The theoretical results are listed in Table I .

Before measuring the self and mutual capacitances of the capacitive coupling interface, the relationship between these parameters and port voltage/current needs to be established. Assuming that an ac current source with amplitude I_s and frequency f is connected to the sth port of the coupling interface, and the other ports are open circuit, (7) can be rewritten as

$$\begin{cases} \mathbf{U}_s = 1/j\omega C_{ss}^* \cdot \mathbf{I}_s \\ \mathbf{U}_t = 1/j\omega C_{st}^* \cdot \mathbf{I}_s. \end{cases} \tag{13}$$

From (13), the following two conclusions can be drawn. First, when all other ports are open, the impedance of port s is equal to the self-capacitance reactance of this port. Second, (13) can further be simplified as follows:

$$C_{st}^* = |\mathbf{U}_s/\mathbf{U}_t| \cdot C_{ss}^*. \tag{14}$$

It means the mutual capacitance C_{st}^* of port s and t can be obtained by connecting a sinusoidal voltage source at port s and measuring the voltage amplitude of port t.

The self and mutual capacitances of the MIMO capacitive coupling interface can be obtained by theoretical calculation,

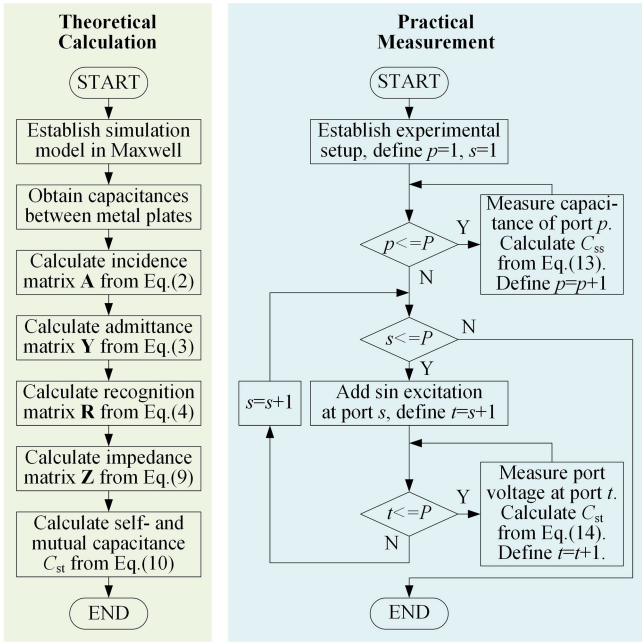

Fig. 6. Flowchart of the theoretical calculation and practical measurement.

including finite-element simulation and practical measurement. The flowchart of the two methods is shown in Fig. 6. For the theoretical calculation, the capacitances between metal plates are obtained from a simulation model established in Maxwell. Then three matrices **A**, **Y,** and **R** can be given from (2)–(4). Then the impedance matrix **Z** of the MIMO capacitive coupling interface can be derived from (9). Finally, the self and mutual capacitances are found from (10). For the practical measurement, all the capacitances of the ports can be measured by an *LCR* meter when all the ports are open and the self-capacitance equal the measured port capacitances according to (13). Then a sinusoidal voltage excitation is connected with the port p, where $p \in [1, P]$, and the voltage of all other ports are measured. The mutual capacitances between any two ports can be derived from (14). The two traversal processes are implemented by loops in the flowchart.

In order to measure the self-capacitance of the coupling interface, accurate *LCR* meter Agilent E4980A is used. Then, a sinusoidal ac voltage source with the amplitude of 10 V and frequency of 1 MHz is connected up to the ports 1–4 successively, as shown in Fig. 7. The open-circuit voltage of other ports is measured and illustrated in Fig. 8. According to (14), the mutual capacitance of the coupling interface can be calculated. All the practically measured values of the self and mutual capacitances of the coupling interfaces are listed in Table I. It should be noted that three mutual capacitance values can be obtained from each of the figures in Fig. 8 and the average value of them is taken as the practical value to compare with the theoretical result.

In Table I, the corresponding theoretical and measured values of self and mutual capacitances were compared and found to be relatively consistent with a maximum error of 6.4%. In Table I, the errors of C_{13} and C_{34} are slightly larger than the others, which may be caused by relatively larger positioning errors of P_5 and

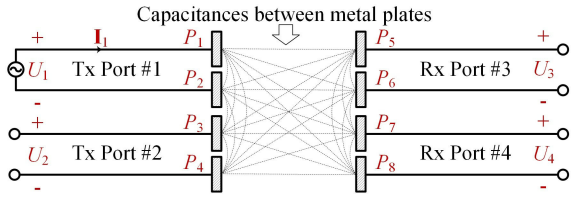

Fig. 7. Structure of the two *Tx* and two *Rx* ports capacitive coupling interface.

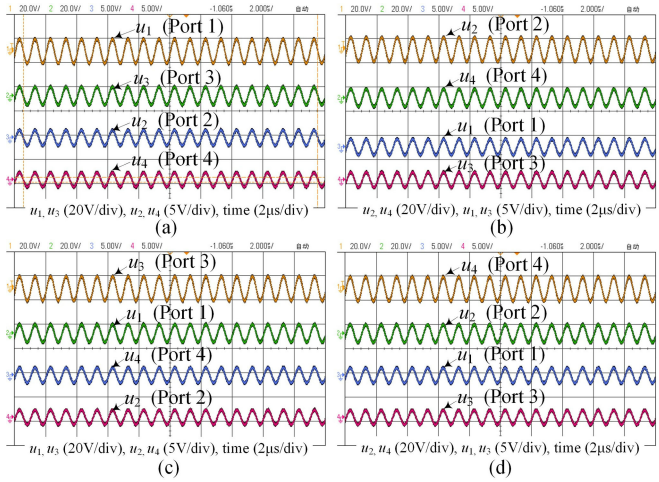

Fig. 8. Experimental waveforms of the opencircuit voltage on each port when a sinusoidal ac voltage source is connected up to (a) port 1, (b) port 2, (c) port 3, and (d) port 4.

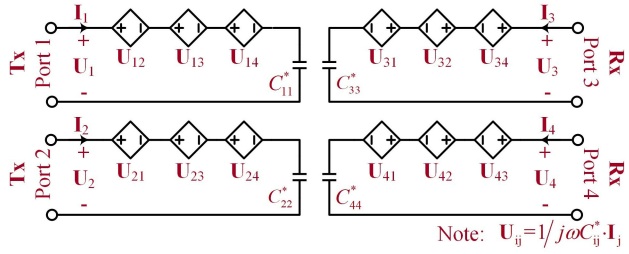

Fig. 9. Equivalent circuit of the two *Tx* ports and two *Rx* ports capacitive coupling interface.

P_6 in the practical experimental setup. For general discussion, the errors between the theoretical and measured capacitances can also be caused by the following reasons: finite-element simulation error; dimension error of coupler; and measurement error. Finally, the circuit of the capacitive coupling interface with two *Tx* and two *Rx* ports is simplified as the equivalent circuit in Fig. 9 according to the proposed mutual coupling model.

IV. Conclusion

This letter introduces a general mutual capacitance model for describing MIMO capacitive coupling interfaces with an arbitrary number of ports. In this model, the self-capacitance of each port and mutual capacitances between any two ports are defined by taking all the capacitances between metal plates into account. An equivalent circuit of the coupling interface is developed, which greatly reduces the complexity of the coupling interfaces. An example capacitive coupling interface setup with two input ports and two output ports is built, and all the self and mutual capacitances of the coupling interface are measured and compared with model-based theoretical values. It is found that the maximum difference between the theoretical and measured values is 6.4%, which is reasonable considering the practical measurement errors. The proposed model can be used for simplifying the analysis of the MIMO capacitive coupling interface and the power transfer performance of MIMO-CPT systems.

References

[1] Y. D. Chung, C. Y. Lee, W. S. Lee, and E. Y. Park, "Operating characteristics for different resonance frequency ranges of wireless power charging system in superconducting maglev train," *IEEE Trans. Appl. Supercond.*, vol. 29, no. 5, Aug. 2019, Art. no. 3602405.

[2] Y. Li *et al.*, "Efficiency analysis and optimization control for input-parallel output-series wireless power transfer systems," *IEEE Trans. Power Electron.*, vol. 35, no. 1, pp. 1074–1085, Jan. 2020.

[3] X. Dai, J.-C. Jiang, and J.-Q. Wu, "Charging area determining and power enhancement method for multiexcitation unit configuration of wirelessly dynamic charging EV system," *IEEE Trans. Ind. Electron.*, vol. 66, no. 5, pp. 4086–4096, May 2019.

[4] F. Farajizadeh, D. M. Vilathgamuwa, D. Jovanovic, P. Jayathurathnage, G. Ledwich, and U. Madawala, "Expandable N-legged converter to drive closely spaced multitransmitter wireless power transfer systems for dynamic charging," *IEEE Trans. Power Electron.*, vol. 35, no. 4, pp. 3794–3806, Apr. 2020.

[5] M. Fu, H. Yin, M. Liu, Y. Wang, and C. Ma, "A 6.78 MHz multiple-receiver wireless power transfer system with constant output voltage and optimum efficiency," *IEEE Trans. Power Electron.*, vol. 33, no. 6, pp. 5330–5340, Jun. 2018.

[6] C. Cheng *et al.*, "A load-independent LCC-compensated wireless power transfer system for multiple loads with a compact coupler design," *IEEE Trans. Ind. Electron.*, vol. 67, no. 6, pp. 4507–4515, Jun. 2020.

[7] J. Dai and D. C. Ludois, "A survey of wireless power transfer and a critical comparison of inductive and capacitive coupling for small gap applications," *IEEE Trans. Power Electron.*, vol. 30, no. 11, pp. 6017–6029, Nov. 2015.

[8] H. Zhang, F. Lu, and C. Mi, "An electric roadway system leveraging dynamic capacitive wireless charging: Furthering the continuous charging of electric vehicles," *IEEE Electrific. Mag.*, vol. 8, no. 2, pp. 52–60, Jun. 2020.

[9] Y.-G. Su, S.-Y. Xie, A. P. Hu, C.-S. Tang, W. Zhou, and L. Huang, "Capacitive power transfer system with a mixed-resonant topology for constant-current multiple-pickup applications," *IEEE Trans. Power Electron.*, vol. 32, no. 11, pp. 8778–8786, Nov. 2017.

[10] F. Lu, H. Zhang, and C. Mi, "A review on the recent development of capacitive wireless power transfer technology," *Energies*, vol. 10, no. 11, Nov. 2017, Art. no. 1752.

[11] C. Liu, A. P. Hu, B. Wang, and N.-K. C. Nair, "A capacitively coupled contactless matrix charging platform with soft switched transformer control," *IEEE Trans. Ind. Electron.*, vol. 60, no. 1, pp. 249–260, Jan. 2013.

[12] L. Huang and A. P. Hu, "Defining the mutual coupling of capacitive power transfer for wireless power transfer," *Electron. Lett.*, vol. 51, no. 22, pp. 1806–1807, Oct. 2015.

[13] H. Zhang, F. Lu, H. Hofmann, W. Liu, and C. C. Mi, "Six-plate capacitive coupler to reduce electric field emission in large air-gap capacitive power transfer," *IEEE Trans. Power Electron.*, vol. 33, no. 1, pp. 665–675, Jan. 2018.

[14] H. Zhang, F. Lu, H. Hofmann, W. Liu, and C. C. Mi, "A four-plate compact capacitive coupler design and LCL-compensated topology for capacitive power transfer in electric vehicle charging application," *IEEE Trans. Power Electron.*, vol. 31, no. 12, pp. 8541–8551, Dec. 2016.